

A computer simulation study of Hertzian cone crack growth

B. R. LAWN*, T. R. WILSHAW AND N. E. W. HARTLEY

Division of Materials Science, School of Applied Sciences, University of Sussex, Falmer, Brighton, England.

(Received, August 9, 1972)

ABSTRACT

A general method for simulating on a computer the growth of the cone-shaped fracture that forms under Hertzian contact loading is outlined. The program involves an incrementing procedure in which both contact circle and cone crack are grown in piecewise manner, according to suitable rate equations. The contact circle expands at a rate determined by the mode of indenter loading, and thereby sets up a time-varying stress field. Appropriate fracture-mechanics criteria are then invoked to calculate the response of the growing crack to the contact stresses. Effects of loading mode, specimen environment and temperature, size and location of the initial flaw from which the cone crack nucleates, are investigated systematically. The computer predictions compare favourably with available experimental data. The results are discussed in the light of previous theoretical treatments of the Hertzian fracture problem, and some new features in the crack-growth characteristics are pointed out. Calculations are made specifically for normal contact loading on glass, but ready extension of the program to other loading situations and materials is envisaged.

1. Introduction

The response of highly brittle solids to the type of stress field induced by forcing two curved surfaces into mutual contact has many theoretical and practical implications. Under critical conditions the response is readily apparent as the sudden appearance of a small crack in one of the solids. The conditions for crack growth depend on the state of the near-surface material, the presence of microcracks (which act as nucleation centres for the macroscopic cracks), residual stresses, and the chemical environment. The size and location of the induced fracture are determined by the geometry of the elastic contact. Of the various possible contact configurations the most convenient is that of a hard sphere (indenter) loaded onto a flat surface (specimen), in which case the induced crack takes the form of a truncated cone. This arrangement forms the basis for the so-called Hertzian fracture test, now developing as a micro-mechanical probe for measuring the strength properties of strong solids.

The analysis of the growth of the Hertzian fractures must take into account the highly inhomogeneous (but well-defined) stress field beneath the indenter [1, 2]. In recent years a theory of Hertzian fracture, using the approach of "fracture mechanics" to determine crack-growth energetics, has been developed by Lawn and co-workers [3-5]. This theory accounts for many features of the Hertzian test, yet it remains incomplete because of the restrictions imposed by certain assumptions. For instance, the treatment computes the mechanics of crack growth for the case in which the contact geometry remains invariant throughout an experiment. In most test arrangements the indenter load increases monotonically, so that the growing crack experiences a time-varying stress field. Again, for the important case where a chemical environment reacts with stressed bonds at the tip of the growing cone crack, it is necessary to introduce kinetic terms into the theory. The incorporation of such terms is considered analytically intractable at present, and to date only a qualitative description of environmental effects in the Hertzian test has been attempted [6]. In addition, the original theory makes assumptions concerning the location of the cone crack relative to the circle of contact, and the value of the elastic constants of the indented material. Consideration of these points has led to important modifications of the original theoretical predictions [7, 8].

In this paper an attempt is made to obtain a more realistic analysis of Hertzian fracture

* On short leave from the School of Physics, University of N.S.W., Kensington, N.S.W., Australia.

growth by avoiding as far as possible all restrictive assumptions. The added complication in mathematical manipulation is handled by simulating the crack growth on a computer. As with all exercises in computer simulation, our model approaches reality at the expense of physical insight and generality. We are, for example, confined to the examination of a particularly well-studied system, that of crack growth in soda-lime glass in the presence of water. While the computer model provides a basis for testing the validity of a specified crack-extension criterion for such a system, it cannot be used to deduce the form of any such criterion from experimental data. Nevertheless, the model serves to indicate the effects of several important fracture parameters, e.g. indenter load rate, test temperature, surface flaw size, elastic constants, environment-crack interaction constants, etc. The study of these effects confirms many of the conclusions of the previous theory, and reveals several new features in the crack growth not previously appreciated.

2. Background theory

2.1. Hertzian elastic contact

We consider the elastic contact between an indenter of radius r , Young's modulus, E' , Poisson's ratio, ν' , and an isotropic elastic half-space of elastic constants, E , ν , as indicated in Fig. 1. The radius, a , of the mutual contact circle is related to the applied force, P by

$$a^3 = \frac{4}{3}(kPr/E), \quad (1)$$

where k is a dimensionless constant,

$$k = \frac{9}{16}[(1-\nu^2) + (1-\nu'^2)E/E']. \quad (2)$$

The distance of mutual approach of the contacting bodies is given by

$$Z = (4k/3E)^{1/3}(P^2/r)^{1/3}. \quad (3)$$

The above three contact equations are sufficient to specify the loading characteristics for any commonly used indenter loading mode. Although it is usual to monitor P rather than a during an experiment, the latter term is more useful as a characteristic parameter for investigating time-variation effects. This, as we shall show later (section 3), arises because a ready comparison between rates of change of contact radius and crack length affords a useful indication of the relative importance of load-rate and environment-interaction effects.

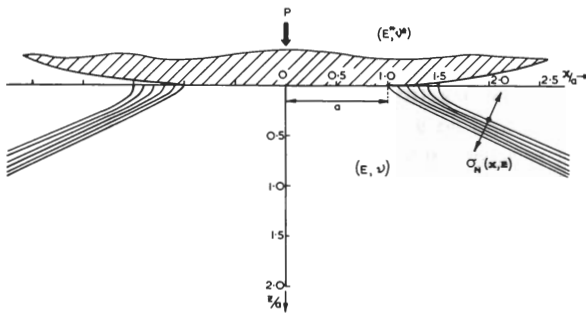


Figure 1. Trajectories of the minimum (most compressive) principal stress under Hertzian contact loading. Calculated for $\nu=0.31$.

We consequently list contact velocities $\dot{a} = da/dt$ for four modes of indenter loading below:

(i) *Constant load rate* ($\dot{P} = dP/dt = \text{const.}$). This mode may be produced by moving a dead weight at constant speed along a cantilever loading arm [9]. Differentiation of (1) with respect to time t gives

$$\dot{a}(a, \dot{P}) = (4kr/9E)(\dot{P}/a^2). \quad (4)$$

(ii) *Constant crosshead speed* ($\dot{Z} = dZ/dt = \text{const.}$). Most standard testing machines operate in this mode. Assuming the machine to be rigid, the crosshead speed is equivalent to \dot{Z} , and we obtain from (1) and (3)

$$\dot{a}(a, \dot{Z}) = r\dot{Z}/2a \tag{5}$$

(iii) *Static load*. The indenter is loaded “instantaneously” to some preselected load and then maintained constant:

$$\begin{aligned} \dot{a} &\rightarrow \infty \quad (-\delta t \leq t \leq 0) \\ \dot{a} &= 0 \quad (0 \leq t \leq t_D), \end{aligned} \tag{6}$$

with $\delta t \ll t_D$, t_D being the duration of loading.

(iv) *Free-fall impact*. For the case where a ball is released under gravity onto a specimen from a height h we have [5]

$$\dot{a}(a, h) = (r^2 gh/2a^2 - 3Ea^2/20\pi k\rho r^2)^{1/2} \tag{7}$$

with $g = 9.80 \text{ ms}^{-2}$, the gravitational acceleration, and ρ the density of the ball (we neglect air resistance).

Figure 2 shows the manner in which \dot{a} varies with a for three modes, the loading parameters being specifically chosen to emphasise the wide range of contact velocities experienced in typical tests. It is pointed out that the contact velocity approaches infinity at initial loading ($a=0$) in all modes above.

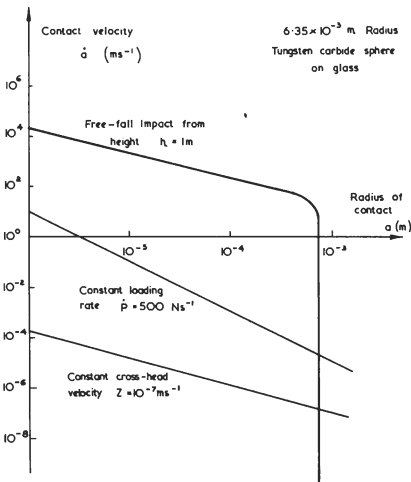


Figure 2. Plots of contact velocity $\dot{a}(a)$ for three specific loading modes. Calculations for tungsten carbide sphere, $r = 6.35 \text{ mm}$, on glass, $E = 7.0 \times 10^{10} \text{ Nm}^{-2}$, $k = 0.55$.

The mechanics of crack growth are determined by the distribution of stresses beneath the indenter. Expressions for the stress components; from a solution by Huber [2], are summarised in the Appendix. The nature of the Hertzian stress field, with particular reference to the fracture behaviour, has been discussed in depth elsewhere [3, 4, 10] and we point out only the essential features here:

- (i) Within a drop-shaped zone beneath the contact circle all principal stresses are compressive.
- (ii) The tensile stress reaches its maximum at the contact circle, and falls off relatively slowly with increasing radial distance from the contact centre along the specimen surface.
- (iii) The tensile stresses decrease rapidly with depth below the specimen surface, the stress gradient being steepest close to the contact circle. This is shown in Fig. 3, in which is plotted the variation of the stress component normal to the plane $x = 500 \mu\text{m}$ with depth z , for several values of the contact radius a .

(iv) The trajectories of the minimum (most compressive) principal stresses start orthogonal to the specimen surface and rapidly deviate outward from the contact circle to form a family of near-parallel curves (Fig. 1) closely resembling the shape of the cone cracks [3]. The stresses normal to these trajectories then represent the greatest of the principal stresses. This component of stress always remains tensile, but shows a tendency to steep gradients not unlike that in Fig. 3 [10].

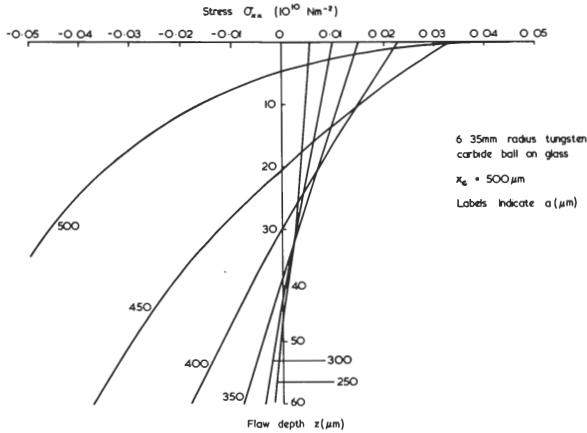


Figure 3. Plots of normal stress $\sigma_{xx}(z)$ along perpendicular surface flaws. Calculated for $x_c = 500 \mu\text{m}$ for several values of contact radius a (labelled).

2.2. Mechanics of crack growth

The surface of a brittle solid generally contains a wide distribution of microcrack sizes. Since cone cracks initiate at such microcracks, tests on as-received surfaces may not be highly reproducible. It is, however, possible to greatly improve reproducibility by uniformly abrading the specimen surface [5]. This action introduces a high density of surface microcracks, whose maximum depth may subsequently be measured to an accuracy of about one micron. When a sphere is loaded onto an abraded surface, a critical stage will be reached at which one of the microcracks will suddenly extend and develop into a full cone crack. *The critical load required to initiate this visible event may be taken to quantify the fracture behaviour.*

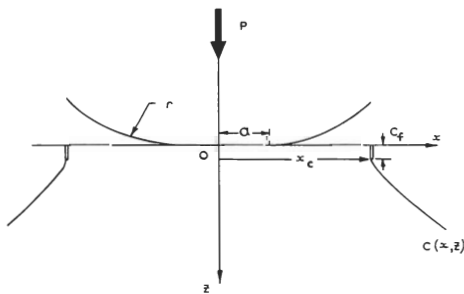


Figure 4. Hertzian fracture parameters.

The basis for a theoretical model of the crack growth behaviour may be outlined with reference to Fig. 4. We consider the growth history of a crack, length c , initiating from a perpendicular flaw, length c_f , located at $(x_c, 0)$ in the specimen surface. The object of the fracture model is to quantitatively describe in detail the growth behaviour, taking into particular account the conditions of indenter loading and the effects of any chemical environment. We then seek the value of x_c which optimises the critical conditions.

In setting up a criterion to determine the conditions of crack extension we use the fracture-mechanics approach previously described [3], approximating the fracture behaviour as follows:

(i) The flaw first propagates around the circle of contact, and subsequently grows downward into the material as a surface "ring" [3, 4, 11].

(ii) The downward-propagating surface crack is approximated by a plane edge crack. This representation is valid only for $c \ll a$, i.e. in the region where crack curvature may be neglected. (The inability to take into account the effects of crack curvature provides the main obstacle to an exact description of the fracture mechanics.)

(iii) The crack path at any instant follows the direction of the principal stress trajectory (Fig. 1) passing through the crack tip [3]. (In the general case of a time-varying stress field the stress trajectory pattern will not remain constant, so that a growing crack will inevitably experience a small component of shear across its interface. However, the shear components will usually be small, and we consider only the effects of tensile stress on crack growth.)

With these points in mind we define the stress intensity factor

$$K = 2(c/\pi)^{\frac{1}{2}} \int_0^c \frac{\sigma(b) db}{(c^2 - b^2)^{\frac{1}{2}}} \tag{8}$$

and the associated crack extension force

$$G = (1 - \nu^2) K^2 / E, \tag{9}$$

with b the distance along the crack, and $\sigma(b)$ the normal stress distribution as determined from the Appendix. Both K and G refer to unit width of crack front.

In the absence of environmental effects the condition for crack extension may be suitably expressed in terms of the Griffith equilibrium equation [13]

$$G = 2\gamma, \tag{10}$$

where γ is the energy of unit area of new fracture surface. However, at temperatures above absolute zero, thermal activation processes may disturb the equilibrium at the crack tip, and the fracture criterion may require to be expressed in terms of rate-dependent equations. We then seek a *kinetic* equation for the rate of crack growth $\dot{c} = v$ (G , or K), in which the fracture mechanics parameters determine the crack velocity. While the essential form of the crack velocity equations may be deduced from rate theory, theoretical understanding of the mechanisms at the crack tip is incomplete, with the result that the parameters in the equations need to be determined empirically for a given system.

The system glass-water has recently been studied over a wide range of values of K and G [14–16]. In these studies several regions of growth behaviour are distinguished:

(i) *Terminal velocity.* At crack velocities approaching near-sonic values, the inertia of the crack walls limits the extension [16]:

$$v_1 \simeq 1500 \text{ ms}^{-1} \tag{11}$$

This region corresponds to large G , K values ($G \gg 2\gamma$), depicted as region I in Fig. 5.

(ii) *Thermally-activated bond rupture.* Beyond the Griffith equilibrium point and below the terminal velocity region, the crack velocity is, in the absence of a chemical environment, determined by the rate at which thermally-activated bond breaking exceeds bond remaking. Except near to the equilibrium, bond-breaking dominates, and the velocity equation [14] (with R the gas constant, T the temperature)

$$v_{II} = 2.0 \times 10^{-3} \exp \left(\frac{-2.58 \times 10^5 + 0.34K}{RT} \right) \tag{12}$$

applies (region II in Fig. 5), all units being in S.I.

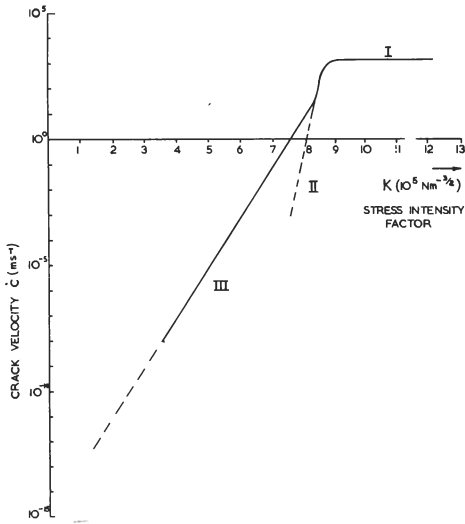


Figure 5. Plots of crack velocity $\dot{c}(K)$ in glass. Curve I–II corresponds to vacuum conditions, curve I–II–III to water (l) environment.

(iii) *Reaction-controlled velocity.* In addition to the above effects, any chemical environment may react with bonds at the crack tip to enhance growth. This process may again be represented by a thermal activation equation [14]:

$$v_{\text{III}} = 2.269 \times 10^4 \exp \left(\frac{-1.088 \times 10^5 + 0.11 K}{RT} \right) \quad (13)$$

(region III in Fig. 5).

The full curve shown in Fig. 5, which fits the data in refs. 14–16 reasonably closely, is artificially generated from the composite relationship

$$\dot{c} = \frac{v_{\text{I}}(v_{\text{II}} + v_{\text{III}})}{v_{\text{I}} + v_{\text{II}} + v_{\text{III}}}. \quad (14)$$

In some systems, in particular when the environment consists of a dilute gas, a further (diffusion limited) region, may be identified between regions II and III [14, 15].

3. The computer model

In the previous section we used the time derivatives of the linear dimensions a and c to respectively characterise the rates of loading and crack growth. Comparison of \dot{a} and \dot{c} then affords a convenient and simple means for assessing the rate-controlling factor in a given Hertzian test: for example, while $\dot{a} \gg \dot{c}$, the load rate may be considered too rapid to allow significant environmental effects to manifest themselves. Some idea of the conditions under which either one or other of the two terms \dot{a} or \dot{c} dominates may be inferred by comparing Figs. 2 and 5.

Considerations of this type are of prime importance when setting up an incrementing procedure to simulate cone crack formation. The logical sequence of steps in our calculation is outlined in the flow chart of Fig. 6. We begin with zero contact and follow the subsequent growth of a surface ring as the indenter is loaded. A suitable choice of increment size is made for both contact and crack, bearing in mind the conflicting demands of accuracy and machine-time cost. We adopt the procedure of using x_c (Fig. 4) as a characteristic length, and impose a maximum number of steps, N , for either a or c to reach this length; N is then adjusted by trial. It is preferable to include some device for allowing the Δa increments to become progressively smaller as the contact circle approaches x_c , and the Δc increments to become likewise larger, since the

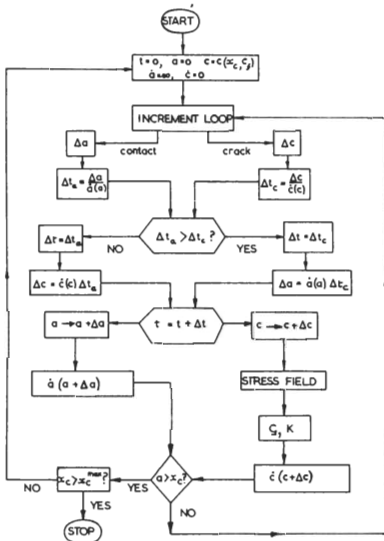


Figure 6. Computer flow chart.

most interesting regions of crack growth are found to occur for $a \rightarrow x_c, c \ll x_c$.

Thus in the first cycle of the incrementing loop we assign tentative values to $\Delta a, \Delta c$, and test for rate control as follows. We compute the corresponding time intervals

$$\Delta t_a = \Delta a / \dot{a}(a), \quad \Delta t_c = \Delta c / \dot{c}(c), \tag{15}$$

and select the smaller as our time increment. This then necessitates a reevaluation of either Δa or Δc , according to whether Δt_a is greater or lesser than Δt_c . Initially, when $\dot{a} \gg \dot{c}$, the contact velocity determines the incrementing step size, whereas as the contact circle expands toward x_c and causes the crack to accelerate, the crack velocity becomes the controlling factor. This scheme has two major advantages: (i) it safeguards against excessive increment sizes (as, for example, could occur at large \dot{c} if we were to fix Δa , compute $\Delta t = \Delta a / \dot{a}$, and then determine the crack increment according to $\Delta c = \dot{c} \Delta t$); (ii) it provides a convenient output in which the interesting regions of rapid crack growth ($a \sim \text{const.}$) or crack arrest ($c \sim \text{const.}$) may be noted at a glance.

After incrementing the contact circle and crack length new values of \dot{a} (equations 4–7) and \dot{c} (equations 8–14) are evaluated for the next cycle. The loop continues until the contact circle encompasses x_c , at which point the crack is placed in compression and ceases to grow. The entire operation is then repeated for a new value of x_c .

4. Results

4.1. Calibration of program output

The program output specifies the growth of the cone crack with time. The purpose of this section is to indicate the manner in which the program parameters need to be adjusted to reconcile prediction with observed behaviour. This adjustment is achieved by forcing the output data to match the results of calibration test runs, made on 12.35 mm thickness abraded glass slabs with a 6.35 mm radius tungsten carbide sphere in vacuum. The data might equally well be reconciled with results from surfaces in their as-received state, but this would involve the added complication of the statistical distribution of size and location of surface microcracks. As we shall see, the sensitivity of the calculation to small variations in input data and theoretical detail leads to some uncertainty in results.

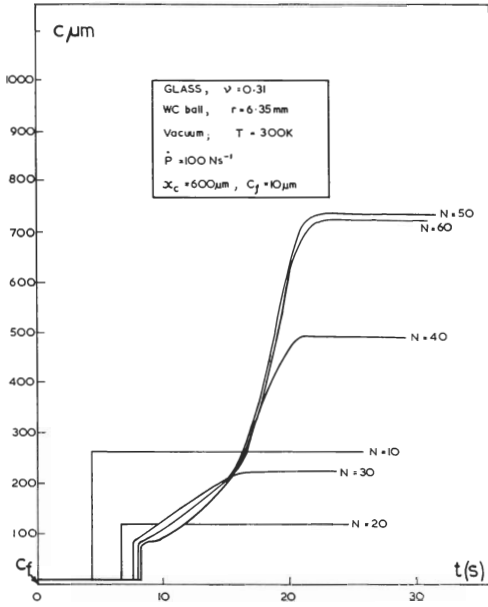


Figure 7. Computer output $c(t)$ for parameters shown inset. Curves for various increment parameters, N .

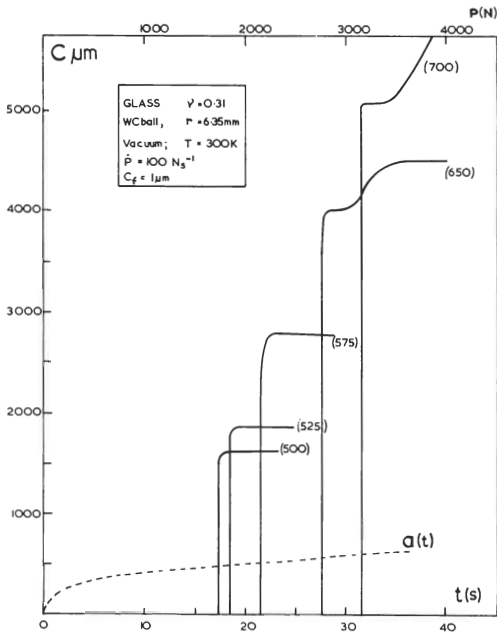


Figure 8. Computer output $c(t)$ for parameters shown inset. Curves for various x_c (labelled). $a(t)$ also shown.

We illustrate first some typical output data in Figs. 7 and 8. These curves are computed for room temperature, vacuum conditions, with a uniform load rate $\dot{P} = 100 \text{ N s}^{-1}$ and elastic constants $E = 7.0 \times 10^{10} \text{ Nm}^{-2}$, $\nu = 0.31$, and $k = 0.55$. Fig. 7 shows the effect of varying the increment-size parameter, N , for the case where $c_f = 10 \text{ } \mu\text{m}$ and $x_c = 600 \text{ } \mu\text{m}$. It is seen that $N = 50$ represents a suitable optimum, and is consequently used in all subsequent calculations. The curve corresponding to this value in Fig. 7 indicates a spontaneous growth of the cone crack from $c_f = 10 \text{ } \mu\text{m}$ to $c \sim 80 \text{ } \mu\text{m}$ at $t \sim 8 \text{ s}$, followed by a rapid, stable phase of downward growth as the loading continues. In this case it is not immediately clear as to the nature of the "critical visible event".

Figure 8 shows the effect of varying x_c , this time for the case $c_f = 1 \mu\text{m}$. Flaws at $x_c \leq 480 \mu\text{m}$ are encompassed within the compressive zone of the Hertzian stress field before they have a chance to become critical. On the other hand flaws further distant from the contact centre propagate unstably to a length of order millimetres, whence they become stable. Further increase in loading causes continued stable extension of the crack, until the surface trace of the cone is “swallowed up” by the advancing contact circle. In Fig. 8 we choose the crack starting at $x_c = 500 \mu\text{m}$ as the one which corresponds to the observed critical event, this being the first crack to become critical. Of course, once this crack begins to propagate, the stress-relieving effect on the neighbouring flaws will tend to suppress multiple cone-crack nucleation; that is, the first crack to become critical will grow at the expense of the others, until the contact “swallows up” the surface trace and allows the stress field to build up once again. We thus note in Fig. 8 that a critical load $P_c \approx 1700 \text{ N}$ is reached after $\approx 17 \text{ s}$ loading time, at which instant $a = 475 \mu\text{m}$, i.e. $a/x_c = 0.95$ at critical loading.

4.2. The effect of Poisson's ratio

In all cases studied the fully developed cone crack tends to follow closely the stress trajectory pattern shown in Fig. 1. This correspondence between predicted and observed crack path is shown in Fig. 9. There is, however, a significant discrepancy. The calculated angle between cone crack and specimen surface for the parameters used in computing the curves in Figs. 7 and 8 is $\approx 26^\circ$, whereas the observed angle for soda-lime glass is closer to $\approx 22^\circ$. If we use a value of Poisson's ratio more representative of the values usually quoted for glass, $\nu = 0.20\text{--}0.25$, the computed crack angle exceeds 30° , thereby worsening the discrepancy. We have to use a Poisson's ratio $\nu \approx 0.33$ to obtain satisfactory agreement.

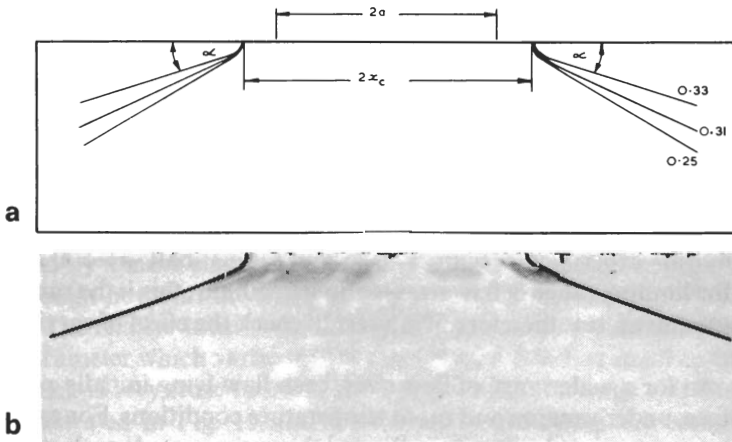


Figure 9. Cone crack paths in glass. (a) Stress-trajectory pattern, for three values of ν (labelled). (b) Observed profile, obtained by section-and-etch through contact symmetry plane [11].

In fact Poisson's ratio has a profound influence on the entire stress field. We illustrate this with reference to Fig. 10, which shows the sensitivity of the “critical fracture load” to variations in ν . In this figure the calculations are for vacuum, room-temperature conditions, with $c_f = 10 \mu\text{m}$. The data are deduced from curves of the type shown in Fig. 7 for $N = 50$. Since a “critical load” is not clearly defined in Fig. 7, we indicate the loads necessary to produce crack lengths in the visibly detectable regime, i.e. cracks of order $100 \mu\text{m}$ in length. Now control tests on glass specimens under the conditions specified above show a sudden crack growth from $c_f = 10 \mu\text{m}$ to $c \approx 1 \text{ mm}$ at a critical load $P_c = 1050 \pm 100 \text{ N}$. Accurate comparison between predicted and observed behaviour is therefore difficult, but the results in Fig. 10 are nevertheless sufficient to show that “realistic” values of Poisson's ratio give fracture loads which are much too small.

On the basis of crack angle and fracture load considerations we are led to choose $\nu = 0.31$

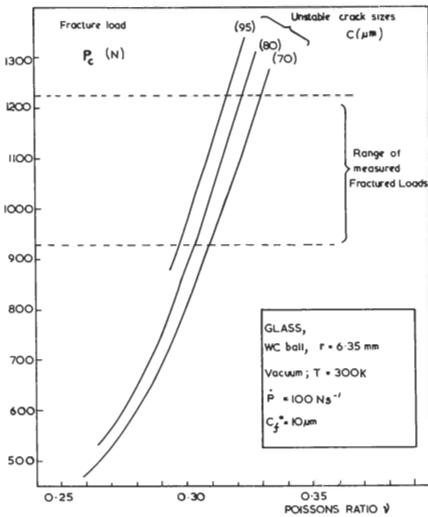


Figure 10. Effect of Poisson's ratio on fracture load. The different curves indicate the load required to produce a cone crack of specified length (labelled).

as an "effective" Poisson's ratio for our calculations on soda-lime glass. This then acts as a "calibration" of the program output. We are aware that this approach is not entirely satisfactory, and indicate possible reasons for the uncertainty surrounding Poisson's ratio in the Discussion. However, while this uncertainty in program parameters rules out the prediction of *absolute* fracture loads, it does not preclude the prediction of *relative* values. The simulation procedure is therefore well suited to investigating the effects of such fracture variables as initial flaw size, load rate, temperature, etc., under specified environmental conditions.

4.3. Effect of initial flaw size

One of the significant predictions of the previous, analytical treatments of Hertzian fracture theory [3–5] was that the critical fracture load should be proportional to indenter radius (Auerbach's law), but *independent of flaw size*, as long as the flaws lay within the size range $4 \times 10^{-3} a \ll c_f \ll 1 \times 10^{-1} a$. In our experiments with a 6.35 mm radius ball $a \approx 500 \mu\text{m}$ typically at critical loading, so the limiting range of flaw sizes is about 2–50 μm ; this is the range normally covered by abraded specimens. It is therefore of interest to check the effect of varying c_f in the computer simulation.

Programs were accordingly run for a wide range of flaw sizes, each flaw lying initially perpendicular to the specimen surface, under vacuum and room temperature conditions. For each value of c_f the location parameter x_c was varied systematically, and the optimum value selected. The results, with appropriate values of c_f and x_c indicated, are shown in Fig. 11. One feature is immediately noticeable; as c_f increases the critical event becomes less distinct, and the crack tends to grow downward in more stable fashion. Adopting as a criterion for fracture the load required to produce a crack size of 90 μm or greater, we predict the smooth curve shown in Fig. 12.

Tests on glass slabs abraded with different grit sizes have recently been performed under vacuum (10^{-6} torr) conditions [17]. The results are indicated by the data points in Fig. 12. Each point represents the mean value and standard deviation, of three separate runs, each on a different specimen, with ten results per run. Experiment and theory show the same trend. The independence of fracture load with flaw size is closely but not exactly respected, noticeable deviations in behaviour occurring at the limits of the flaw size range. Of special interest is the observation that larger flaws become *less* severe as c_f exceeds $\approx 10 \mu\text{m}$. Close inspection of the critical event in the experiments showed that the more heavily abraded surfaces are character-

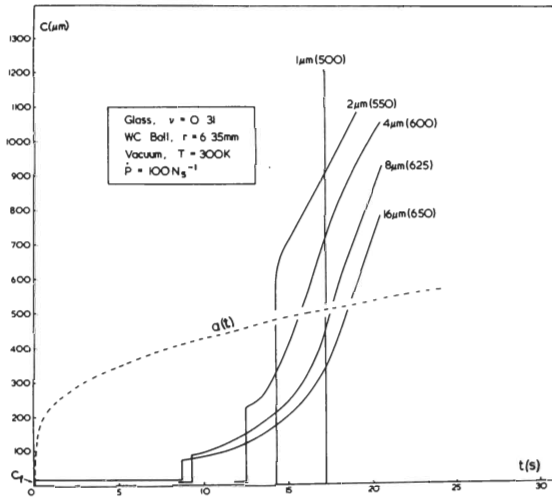


Figure 11. Effect of initial flaw size on growth of cone cracks. Labels indicate values of c_f and optimum x_c (parentheses).

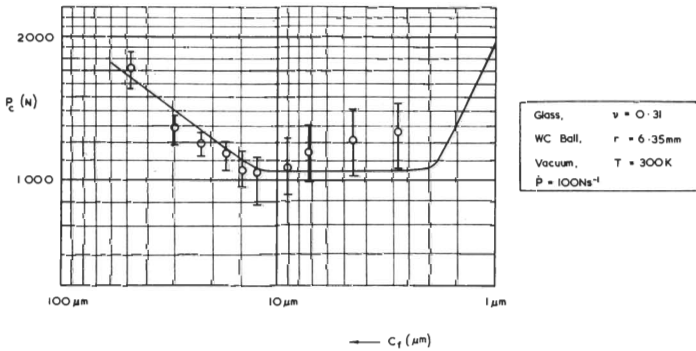


Figure 12. Variation of fracture load with initial flaw size. Smooth curve indicates computer prediction, data points indicate vacuum test results. (Data courtesy A. G. Mikosza and J. J. H. Beek).

ised by a more sluggish growth to the fully developed cone, in accordance with the trend (although not with the scale) in Fig. 11.

The relative location of critical contact circle and surface trace of the cone crack is another parameter which varies with the initial flaw size. For small c_f the point of initiation of the cone crack is very close to the contact circle, while for large c_f it lies well outside. This tendency is illustrated in Fig. 13, the smooth curve indicating the computer predictions and the data points indicating experimental values [17].

4.4. Effect of load rate and environment

In an earlier paper [6] it was shown that the presence of a reactive environment could have a profound influence on the Hertzian strength. Computer simulations have accordingly been made of cone crack growth in glass in the presence of water. In all cases the flaw size has been fixed at $c_f = 10 \mu\text{m}$, and the crosshead speed \dot{Z} used as computer variable. Figs. 14 and 15 show a selection of crack growth families for $\dot{Z} = 1 \text{ ms}^{-1}$ and 10^{-6} ms^{-1} respectively, with $T = 300 \text{ K}$. It is seen that the general shape of the curves is similar in both cases, with a slight tendency for the slower load rate to produce an even more sluggish development of the cone than before. There is, however, a significant difference of a factor of two in the magnitude of the fracture load in the respective cases.

Fig. 16 shows the variation of load with the load duration at critical fracture (defined as in

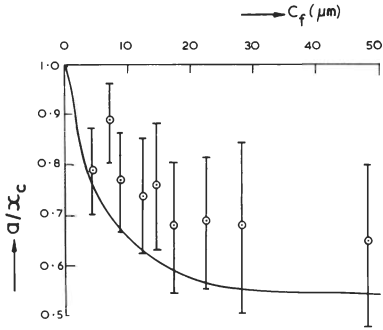


Figure 13. Plot showing relative locations of contact circle and surface ring crack as function of flaw size (from vacuum computations). (Data courtesy M. V. Swain).

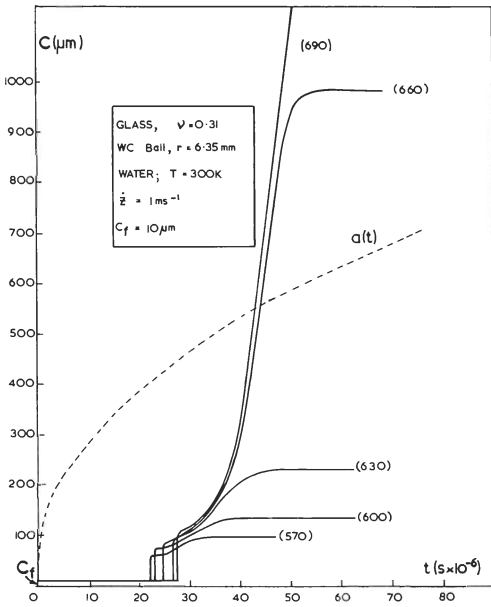


Figure 14. Computer output $c(t)$ for parameters shown inset. Curves for various x_c (labelled). $a(t)$ also shown.

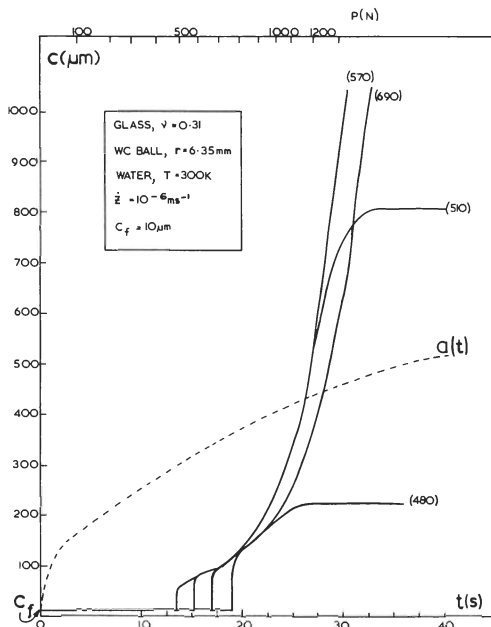


Figure 15. As for Fig. 14, but with crosshead speed reduced by factor of 10^6 .

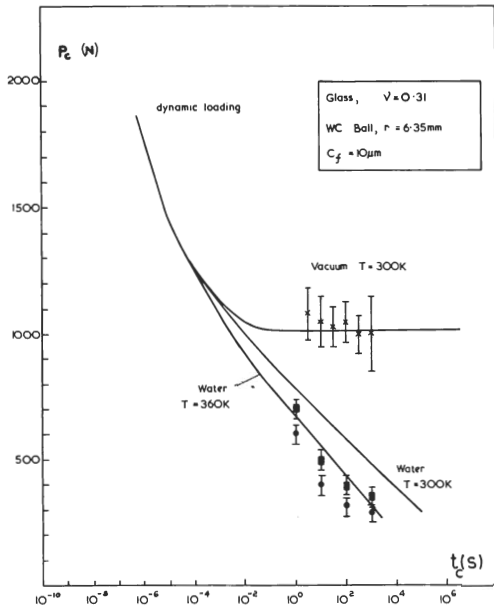


Figure 16. Variation of fracture load with load duration and environment. Smooth curves indicate computer predictions, data points indicate test results in water [6] [$T = 300$ K (squares), $T = 360$ K (circles)] and vacuum (data courtesy J. J. H. Beek and M. V. Swain).

the previous section). For the sake of comparison, curves are shown for cone crack formation in water at $T = 300$ K and 360 K, and in vacuum at $T = 300$ K. Some experimental data [6, 17] are included in Fig. 16; unfortunately these data cover only a small range of loading rates, and are inaccurate at the two extremities of the range covered.

The curves of Fig. 16 show several points of interest. At very fast crosshead speeds, in the region $\dot{Z} \gtrsim 1 \text{ ms}^{-1}$, all curves merge and show a rapid increase in P_c as t_c becomes small. In this region the behaviour is controlled by the load rate, the condition $\dot{a} > \dot{c}$ becoming satisfied throughout the indentation procedure. At these load rates the crack, even when propagating at its terminal velocity, cannot respond quickly enough to the rapidly applied load; in other words, we are operating in a truly dynamical loading regime.

As the crosshead speed is reduced below $\dot{Z} \approx 1 \text{ ms}^{-1}$ the nature of the environment becomes important. The curve representing the vacuum tests levels off, showing only slight decline as the duration of loading is prolonged. On the other hand the tests in water environment show a dramatic plunge over the same time scale. The effect of raising the temperature is apparently to shift the curve to the left along the time ordinate; this leads to substantial reductions in the fracture load, especially at the slower load rates.

Finally, experiment also shows that the diminishing critical load in Fig. 16 is accompanied by more sluggish development of the cone crack [6], and a gradually increasing ratio a/x_c [8]. This is consistent with the computer predictions, although at lower load rates it becomes increasingly difficult to assign a value to the critical contact radius with any confidence (see Fig. 15).

5. Discussion

The comparison of the computer simulation predictions with existing experimental data shows reasonable agreement. However, the uncertainties still inherent in certain aspects of the theory, together with the limitations of available data, indicate the need for further work. Nevertheless, the exercise has value in that it leads to an understanding of such hitherto unexplained features of the Hertzian test as the variation in relative location of contact circle and surface crack,

the transition from abrupt to sluggish development of the cone with increase in flaw size and load duration, etc. In addition, the computer calculations extend into experimentally unexplored regimes, e.g. into the region of dynamic loading in Fig. 16, and thus serve to provide foresight for future experiments.

The most serious shortcoming of the simulation is that it does not predict the scale of the rapid cone crack growth observed in experiments. The practice adopted here of identifying the critical event with the load needed to produce a cone crack of length $90\ \mu\text{m}$ is somewhat arbitrary. It appears that a more rigorous treatment of the fracture mechanics is required, in particular accounting for the energetics of a curved crack; the cone curves more sharply in the initial stages of growth, where the surface ring begins to flare outward along the stress trajectories, and it is in the early stages that the critical conditions are determined. Again, the question should be asked whether or not the Hertzian stress field, calculated on the basis of isotropic, linear elasticity theory, is an adequate representation of reality. In this connection Poisson's ratio becomes an important consideration.

For in cases where nominally isotropic materials, such as glass, fused silica, etc., suffer significant stresses, the elastic behaviour can become non-linear, and Poisson's ratio can vary significantly. Mallinder and Procter [18] measured ν for fused silica by comparing extension and shear moduli, and found increases up to a factor of two at strain levels ≈ 0.05 . The material, initially isotropic, becomes orthotropic under tension as the SiO_4 tetrahedra distort. In our Hertzian tests the maximum strain (compressive) reaches the same level as above. It is therefore not inconceivable that non-linear effects, compounded by the inhomogeneous nature of the stress field, could lead to substantial deviations from ideal Hertzian behaviour. Until such effects can be taken into account we feel that the procedure of adjusting the "effective" Poisson's ratio represents the most suitable means for effecting a calibration of the computer output. We should, however, emphasise that the *trends* predicted by the computer calculations are not sensitive to variations in ν .

The effect of initial flaw size on the critical loading brings out some features of particular interest. As mentioned in section 4.2 the independence of fracture load P_c of flaw size c_f is central to the applicability of the so-called Auerbach law. It is, of course, this very independence of Auerbach's law on the state of the surface damage that makes the Hertzian test attractive, allowing for high reproducibility in results without the need to take excessive care in specimen preparation [5]. The earlier theories [3-5] of Hertzian fracture attributed this feature in the fracture mechanics to an initial stage of stable flaw growth prior to full development of the cone, and there is experimental evidence to support this contention [11]. However, because of the uncertainty of the computer output in the critical early stages of ring-crack growth, there appears to be little chance at present of resolving this particular issue by simulation.

There is, on the other hand, a clear reason for the apparently anomalous result in Fig. 12, in which the fracture load actually *increases* as the flaw size becomes large. Referring to Fig. 3 we see that a flaw lying perpendicular to the specimen surface is subjected to distribution of normal stress which decreases with depth. Small flaws, say $c_f \approx 1-10\ \mu\text{m}$, experience relatively uniform tension along their length, until the contact circle approaches within $\approx 0.9 x_c$. Such flaws, when they extend, will be able to curve away from the orthogonal orientation and outward along the stress trajectories (Fig. 1), thereby maintaining tensile stresses along the entire crack path. On the other hand, larger flaws, i.e. $c_f \gtrsim 10\ \mu\text{m}$, extend into a region of compression at their end, and thus have a tendency to close up. This is, to our knowledge, the first reported instance in which smaller flaws may be more dangerous than larger ones. The argument holds regardless of the initial *orientation* of the flaws; owing to the strong curvature of the stress trajectories near the specimen surface, large inclined flaws would still experience some component of compression along their length.

Yet another aspect of the flaw size factor has its interpretation embodied in the stress distributions of Fig. 3. This concerns the increasing tendency for the cone crack to form remote from the contact circle as c_f increases (Fig. 13). For $c_f \leq 1\ \mu\text{m}$ the flaw suffers near-uniform tension for all $a \leq x_c$, so the tendency will be for the cone to initiate close to the contact circle,

where the tensile stress has its maximum value. However, for say $c_f = 20 \mu\text{m}$ the rapid fall-off in stress as a approaches x_c is not conducive to extension, and the flaw is more likely to grow at $a \approx 0.8 x_c$, where the tension remains reasonably high along the entire length.

As to the effects of load rate and environmental interaction on Hertzian strength the computer predictions serve mainly as a semi-quantitative guide to the different regions of behaviour. Apart from the above-mentioned uncertainties in the Hertzian theory itself the chemical kinetics of the environmental interactions are not well understood, the rate-dependent equations being largely empirical. There is also a lack of experimental data for comparison with the computer predictions, particularly at the extremities of the load-rate range in Fig. 16. Work is currently being carried out in these laboratories on dynamic loading effects, using shock-loading to produce load durations $\ll 10^{-6}$ s [19]. At the other end of the time scale experimentation present some problems, because of the difficulty in identifying a critical fracture load; more work should be done in this area, however, with the aim of investigating the existence or otherwise of a static fatigue limit.

Thus, until the mechanisms of fracture are more clearly established at a fundamental level, the applicability of the simulation method of crack growth is restricted to those materials for which crack velocity data are available. The method is nonetheless useful as a model for testing fracture criteria in contact problems, and, indeed, in any other fracture mechanics problem in which an analytical solution is intractable. It is then a simple step to adapt the case of normal loading considered here to the solution for a sliding indenter [20, 21] and to thereby simulate many of the characteristics of abrasion, erosion, and fragmentation of brittle materials. [22]

Acknowledgements

We are grateful to the following colleagues for providing data for this paper, and for discussions: J. J. H. Beek, A. G. Mikosza, M. V. Swain (University of New South Wales), P. B. Withers, G. M. Crimes, W. Swindlehurst (University of Sussex), and J. Heavens (Pilkington Bros. Laboratories, Lathom). One of us (BRL) wishes to record his gratitude to Professor R. W. Cahn for making provision to work in this laboratory.

Appendix: The elastic stress field

The Hertzian stress field has the property of geometrical similarity if all spatial coordinates are normalised to the contact radius a , and all stresses are normalised to the mean contact pressure $p_0 = P/\pi a^2$. The stresses in the Oxz plane are given by Huber [2] as follows:

$$\frac{\sigma_{xx}}{p_0} = \left(\frac{1-2\nu}{2}\right) \frac{a^2}{r^2} \left[1 - \left(\frac{z}{\sqrt{u}}\right)^3\right] + 1.5 \left(\frac{z}{\sqrt{u}}\right)^3 \left(\frac{a^2 u}{u^2 + a^2 z^2}\right) + 1.5 \frac{z}{\sqrt{u}} \left[(1-\nu) \frac{u}{a^2 + u} + (1+\nu) \frac{\sqrt{u}}{a} \arctan\left(\frac{a}{\sqrt{u}}\right) - 2 \right]$$

$$\frac{\sigma_{zz}}{p_0} = -1.5 \left(\frac{z}{\sqrt{u}}\right)^3 \left(\frac{a^2 u}{u^2 + a^2 z^2}\right)$$

$$\frac{\sigma_{xz}}{p_0} = -1.5 \left(\frac{xz^2}{u^2 + a^2 z^2}\right) \left(\frac{a^2 \sqrt{u}}{a^2 + u}\right)$$

where

$$u = \frac{1}{2} \{ (x^2 + z^2 - a^2) + [(x^2 + z^2 - a^2)^2 + 4a^2 z^2]^{\frac{1}{2}} \}.$$

The principal stresses across the crack path are

$$\sigma_N(x, z) = \sigma_{xx} \sin^2 \alpha + \sigma_{zz} \cos^2 \alpha - 2\sigma_{xz} \sin \alpha \cos \alpha$$

where the angle α between the crack path and specimen surface is found from

$$\tan 2\alpha = -2\sigma_{xz} / (\sigma_{xx} - \sigma_{zz}).$$

REFERENCES

- [1] H. Hertz, *Hertz's Miscellaneous Papers*, Chs. 5 and 6. (MacMillan, London, 1896).
- [2] M. T. Huber, *Ann. Physik*, 14 (1904) 153.
- [3] F. C. Frank and B. R. Lawn, *Proc. Roy. Soc.*, A299 (1967) 291.
- [4] B. R. Lawn, *J. Appl. Phys.*, 39 (1968) 4828.
- [5] F. B. Langitan and B. R. Lawn, *J. Appl. Phys.*, 40 (1969) 4009.
- [6] F. B. Langitan and B. R. Lawn, *J. Appl. Phys.*, 41 (1970) 3357.
- [7] T. R. Wilshaw, *J. Phys. D. Appl. Phys.*, 4 (1971) 1567.
- [8] J. Heavens, unpublished work.
- [9] J. J. H. Beek and B. R. Lawn, *J. Phys. E. Scientific Instrum.*, in press.
- [10] von H. Rumpf and K. Schönert, Third European Symposium on Comminution, Cannes, France, Oct. 5-8, 1971, p. 27-56. Dechema Frankfurt; Verlag Chemie Weinheim.
- [11] A. G. Mikosza and B. R. Lawn, *J. Appl. Phys.*, 42(1971) 5540.
- [12] The stress-intensity factor defined here differs by a factor of $\sqrt{\pi}$ from that used in some other papers.
- [13] A. A. Griffith, *Phil. Trans.*, A221, (1920) 163.
- [14] S. M. Wiederhorn and L. H. Bolz, *J. Amer. Ceram. Soc.*, 53 (1970) 543.
- [15] K. Schönert, H. Umhauer and W. Klemm, *Fracture*, Proceedings of Second International Conference, Brighton, 1969, paper 41.
- [16] F. Kerkhof and H. Richter, *Fracture*, Proceedings of Second International Conference, Brighton, 1969, paper 40.
- [17] A. G. Mikosza, J. J. H. Beek and M. V. Swain, unpublished work.
- [18] F. P. Mallinder and B. A. Proctor, *Phys. and Chem. Glasses*, 5 (1964) 91.
- [19] P. B. Withers, unpublished work.
- [20] G. M. Hamilton and L. E. Goodman, *J. Appl. Mech.*, 33 (1966) 371.
- [21] B. R. Lawn, *Proc. Roy. Soc.*, A299 (1967) 307.
- [22] N. E. W. Hartley, Ph. D. thesis, University of Sussex, 1971.

RÉSUMÉ

On traite d'une méthode générale de simulation sur ordinateur de l'extension d'une rupture en forme de cône, telle qu'il s'en présente lors de mises en charge par contact Hertzien.

Le programme comporte une procédure par incréments, où l'on accroît par pliers le cercle de contact et la fissure conique, en se référant à des équations décrivant adéquatement cette croissance.

La vitesse d'expansion du cercle de contact dépend du mode de mise en charge de l'indentation; elle entraîne la création d'un champ de contraintes variables dans le temps. Les critères appropriés de la mécanique de rupture peuvent alors être invoqués pour calculer la relation liant la dimension de la fissure aux contraintes de contact. On a étudié de manière systématique les effets du mode de sollicitation, de l'environnement et de la température de l'éprouvette, de la dimension et de l'emplacement du défaut initial à partir duquel se forme la fissure conique. Les prédictions fournies par le ordinateur s'accordent bien aux données expérimentales disponibles.

Les résultats sont discutés à la lumière des développements théoriques qui ont déjà été consacrés précédemment au problème de la rupture sous contact Hertzien, et font ressortir des connaissances nouvelles sur les caractéristiques d'extension de ce type de fissures.

En principe, les calculs ont été effectués dans le cas d'une charge normale à une surface de verre, mais on envisage dès à présent une extension du programme à d'autres conditions de charge et à d'autres matériaux.

ZUSAMMENFASSUNG

Man behandelt ein allgemeines Komputerverfahren zur Simulation der Ausbreitung eines konischen Bruches unter hertzischer Kontaktbelastung. Das Programm enthält ein Inkrementverfahren in dem sowohl der Kontaktkreis wie der konische Riß stufenweise erwachsen, in Übereinstimmung mit annehmbaren Ausbreitungsgeschwindigkeitsgleichungen. Der Kontaktkreis hat eine Ausbreitungsgeschwindigkeit die von der Einzahnungsbelastung abhängt, und führt dadurch ein zeitlich veränderliches Spannungsfeld ein.

Dann werden passende Bruchmechanikskriterien angewandt um den Zusammenhang zwischen der Rißausbreitung und der Kontaktspannungen zu rechnen. Einflüsse des Belastungsverfahrens, Umgebung und Temperatur des Prüfstabes. Größe und Lage des Anfangsfehlers von dem der konische Riß ausgeht, werden systematisch untersucht. Die Voraussagen des Computers sind günstig vergleichbar mit den Versuchsergebnissen.

Man bespricht die Resultate im Rahmen von bestehenden theoretischen Lösungen des Hertzischen Bruchproblems, und einige neue Gesichtspunkte in den Rißausbreitungsbegebenheiten werden hervorgehoben.

Die Rechnungen wurden besonders für normale Kontaktbelastung auf Glass aufgestellt, aber schon jetzt werden Ausdehnungen des Verfahrens für andere Belastungen und andere Werkstoffe in Betracht gezogen.